

# Novel Time Domain Radiowave Propagators for Wireless Communication Systems

**F. AKLEMAN**

*ITU Dept. of Electronics and Communication Engineering,  
80626, Maslak, İstanbul-TURKEY  
e-mail: funda@ehb.itu.edu.tr*

**M. O. ÖZYALÇIN**

*ITU Dept. of Electronics and Communication Engineering,  
80626, Maslak, İstanbul-TURKEY  
Turkish Airforce Academy, Dept. of Electronics Eng.,  
34807, Yesilyurt, İstanbul-TURKEY  
e-mail: oozyalcin@hho.edu.tr*

**L. SEVGİ**

*Electronics and Communication Engineering Department, Doğuş University,  
Zeamet Sok. No: 21, Acıbadem/Kadıköy, İstanbul-TURKEY  
e-mail: lsevgi@dogus.edu.tr*

## Abstract

*In this study, novel time domain wave propagators are used in path loss calculations for macro and micro cell coverage planning in wireless communication systems. Both Transmission Line Matrix (TLM) and Finite-Difference Time-Domain (FDTD) based propagators, which were introduced recently and validated and verified on different canonical propagation scenarios, are used for this purpose. Examples are chosen both in rural and urban areas, where two propagators are compared with each other. Excellent agreement between the results obtained via two propagators is presented. The results presented here are very encouraging and these propagators are shown to be powerful tools for not only academic research, but also as precise engineering tools.*

**Key Words:** *Time domain wave propagators, wireless communication systems, FDTD, TLM, terrain effects*

## 1. Introduction

Today's communication and radar systems require powerful propagation prediction tools. While a rough line-of-sight (LOS) analysis may be adequate for most of microwave links and radar systems, accurate propagation prediction is essential for most of emerging systems, such as macro and micro cell planning for cellular communication system, site selection for the emerging high-frequency (HF) and very high frequency (VHF) radar systems, etc. These require simulation of propagation in realistic environments, which include;

- Ground wave propagation over spherical non-flat, imperfect earth's surface including multi-mixed paths (e.g., land-sea, soil-vegetation transitions),

- Boundary layer atmospheric conditions (e.g., temperature fluctuations, pressure variations, etc.) which can be represented via the refractivity of air and may cause guiding, surface trapping, elevated ducting, etc. wave phenomena,
- First order electromagnetic (EM) scattering effects, such as direct arrivals, specular reflections, multi-path delays (i.e., interference),
- Second order EM scattering effects, such as edge and/or tip diffractions, multi-reflections (ringing), surface waves, etc.

Analytic solutions are far from handling most of these effects and available ones are approximate (such as ray, mode methods), limited with simple geometries (smooth, plane earth, concave or edge boundaries, etc.) and valid for only certain parameter regimes (such as in a limited frequency band, for far-field, in highly conductive medium, etc.). There are analytical-numerical techniques in frequency domain, which have been in use for a few decades. For example, split-step parabolic equation (SSPE) has successfully been used in modeling propagation and can handle most of the requirements listed above. But, SSPE is a one-way propagator that neglects backscatter effects and is valid for only near axial propagation problems. Although hybridization of all these analytical and analytical-numerical techniques extends the range of application and validity, emerging communication and radar systems still need new powerful propagation simulators (see [1] for a brief historical overview of the techniques mentioned above).

Recently, two time domain wave propagators, based on two-dimensional (2D) Finite-Difference Time-Domain (FDTD) and Transmission Line Matrix (TLM) techniques have been introduced, validated and verified in various ground wave propagation environments directly in time-domain [2-5]. They are named as Time-Domain Wave-Propagator (TDWP) and Transmission Line Matrix Wave-Propagator (TLM-WP). In this study, TDWP and TLM-WP are used in path loss calculations for macro and micro cell coverage planning in wireless communication systems.

Extensive studies, from empirical models to analytical/numerical formulations, have been carried out on predicting the received radio signal strengths in wireless communication systems. Among the others, a popular one is introduced by Okumura [6], who has published an empirical technique for predicting the field strength and service area for a given terrain of the land mobile radio system (over the frequency range of 150-2000 MHz, in ranges from 1 km to 100 km, and for base station effective antenna heights between 30 m to 1000 m). Okumura's empirical technique depends on the extensive series of measurements in and around Tokyo, Japan. Then, based on Okumura's results, Hata [7] has developed an empirical formula, where propagation loss is easily computable. In the same content, Bullington [8] has introduced a series of nomograms derived from theoretical expressions for radio wave propagation loss calculations. Walfisch and Bertoni [9] have published a theoretical model that considers the effects of buildings on radio propagation, where buildings are assumed as absorbing and diffracting cylinders lying on the earth and propagation process is reduced to multiple forward diffraction over a series of screens. Chan [10] has developed a kind of prediction model, which includes empirical formula as well as analytical approximations in calculating point-to-point path loss. Different 2D or 3D ray-tracing methods have also been developed (e.g., Neve-Rowe [11] model) for propagation prediction in urban areas, considering building effects.

The path loss between a pair of antennas is the ratio of the transmitted power to the received power and it is usually expressed in dB. The received power at the input terminal of the receiver may be expressed as

$$P_R = \frac{P_T G_T G_R}{L_P L_S} [W] \quad (1)$$

where  $P_T$ ,  $G_T$ ,  $G_R$ ,  $L_P$  and  $L_S$  are the transmitted power, transmit antenna gain, receive antenna gain, propagation loss and system losses, respectively. In (1), the antenna gains are expressed with reference to isotropic antenna and  $L_S$  represents all system losses including thermal losses, cable and impedance mismatch losses, etc. The propagation (path) loss can be defined as

$$L_P = \frac{P_T G_T G_R}{P_R L_S} \quad (2)$$

which describes only the propagation medium essentially independent of the system gains and losses. Thus, main goal of propagation simulating is to predict  $L_P$  as accurately as possible, allowing the range of cell coverage, shadow regions, etc., to be determined before installation. Propagation loss  $L_P$  represents all scattering effects; free space loss, multi path interference, obstacle scattering, etc. Therefore, the simulator should be capable of handling all these effects.

## 2. TDWP and TLM-WP

TDWP and TLM-WP radio wave propagators are developed for the classical TM to z problem, which models EM waves excited from a vertical electric dipole located over the ground in 2D rectangular co-ordinate system. The problem and the geometry are pictured in Figure 1. The problem may be radio wave propagation over non-flat, imperfect, spherical earth's surface, above which may exist transversely as well as longitudinally inhomogeneous atmosphere (Figure 1a). Or, it may be a propagation problem along a street of a densely occupied metropolitan area (Figure 1b). Here, necessary field components are  $E_x$ ,  $H_y$  and  $E_z$ , where x and z are chosen as the transverse (height) and longitudinal (range) coordinates, respectively. In this TM to z problem, the propagation region is a semi-infinite region that extends from  $x=0$  (bottom) to  $x \rightarrow \infty$  (top), and from  $z \rightarrow -\infty$  (left) to  $z \rightarrow \infty$  (right). As shown in Figure 1, the difficulty of investigating radio wave propagation via the classical FDTD [12] or TLM [13] techniques is the requirement of observing fields that extends far beyond the computation spaces. This is overcome by tracing the propagation region with a dynamic sliding window. The sliding window (i.e., the computation space) has to be terminated by absorbing boundary blocks from the left, right and top (here perfectly matched layer, PML is used). This is pictured in Figure 2 with both TLM and FDTD unit cells. A one-cell transition is used to match the FDTD field components to the TLM voltage pulses in order to use the same FDTD-based PML routine in both propagators. It should be noted that using the same termination is very important in error analysis.

In TDWP, related FDTD iterative equations;

$$E_x^n(i, k) = \frac{\epsilon}{\epsilon + \sigma \Delta t} E_x^{n-1}(i, k) - \frac{\Delta t}{(\epsilon + \sigma \Delta t) \Delta z} \left[ H_y^{n-1/2}(i, k) - H_y^{n-1/2}(i, k-1) \right] \quad (3)$$

$$E_z^n(i, k) = \frac{\epsilon}{\epsilon + \sigma \Delta t} E_z^{n-1}(i, k) + \frac{\Delta t}{(\epsilon + \sigma \Delta t) \Delta x} \left[ H_y^{n-1/2}(i, k) - H_y^{n-1/2}(i-1, k) \right] \quad (4)$$

$$\begin{aligned}
 H_y^{n+1/2}(i, k) = & H_y^{n-1/2}(i, k) \\
 & - \frac{\Delta t}{\mu_0 \Delta z} [E_x^{n-1}(i, k+1) - E_x^{n-1}(i, k)] \\
 & + \frac{\Delta t}{\mu_0 \Delta x} [E_z^{n-1}(i+1, k) - E_z^{n-1}(i, k)]
 \end{aligned} \tag{5}$$

are used, where  $\epsilon$  [F/m],  $\sigma$  [S/m] and  $\mu$  [H/m] are the permittivity, conductivity and permeability of the propagation medium, respectively (free space permeability,  $\mu_0$  is considered throughout the study). Here,  $i$  and  $k$  are the cell numbers in the  $x$  and  $z$  coordinates, respectively, and  $n$  tags the time step. FDTD electric field components are calculated at discrete time instants  $\Delta t, 2\Delta t, 3\Delta t, \dots, n\Delta t$ , and the magnetic field components are calculated at  $\Delta t/2, 3\Delta t/2, 5\Delta t/2, \dots, (n+1/2)\Delta t$ , in cubical Yee cells [12] with cell sizes  $\Delta x, \Delta y, \Delta z$ . The corresponding TLM components  $I_y, V_x$  and  $V_z$  are determined from Thevenin equivalence of the series node [13]

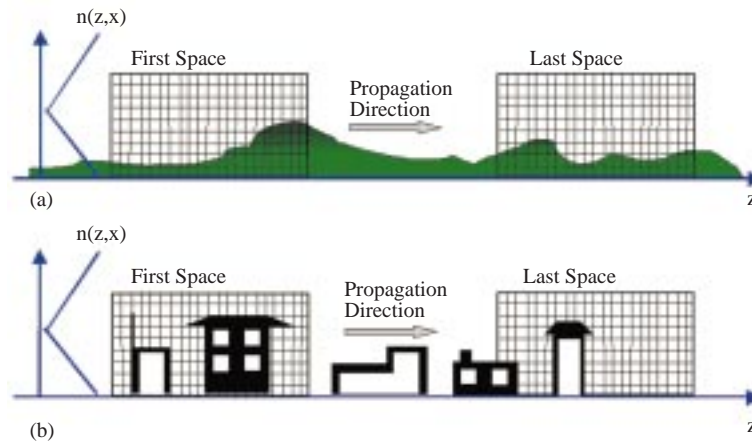


**Figure 1.** The 2D propagation space, (a) non-flat terrain in rural area, (b) buildings along a street (with a vertical bi-linear refractivity profile).

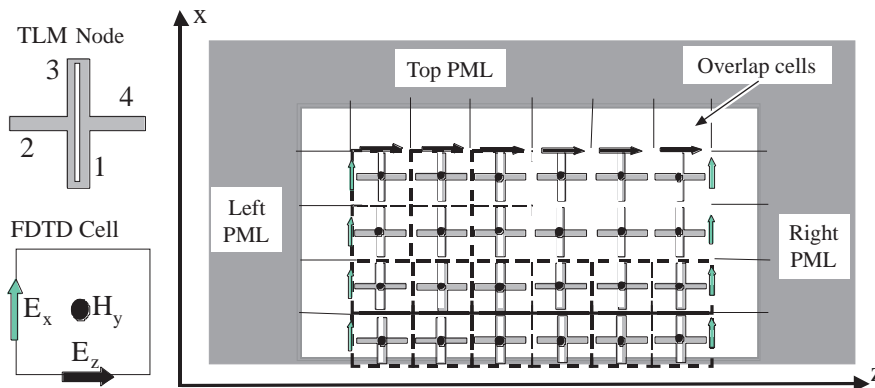


**Figure 2.** TLM, FDTD unit cells and the sliding window bounded by PML blocks. This computation window covers the region by sliding from left to right.

$$H_y = \frac{I_y}{\Delta\ell}; E_x = -\frac{V_x}{\Delta\ell}; E_z = -\frac{V_z}{\Delta\ell} \quad (6)$$

as

$$I_y = 2 \frac{V_1^i - V_2^i - V_3^i + V_4^i + V_5^i}{\hat{Z} Z_{TL} \Delta\ell}; \quad V_x = V_2^i + V_4^i; V_z = V_1^i + V_3^i \quad (7)$$

where  $\hat{Z} = 4 + Z_s$  and  $Z_s = 4(\mu_r - 1)$ . The characteristic impedance of each individual transmission line,  $Z_{TL}$  becomes  $Z_o/\sqrt{2}$ , where  $Z_o$  is the characteristic impedance of the free space. The propagation medium has relative permeability of 1 but the relative permittivity of  $\epsilon_r$ . So, by duality, normalized impedance of the short-circuited stub,  $Z_s$  becomes  $Z_s = 4(\epsilon_r - 1)$ , meaning that the short circuited stub models the permittivity of the medium.

The implementation of non-flat perfectly electrical conductor (PEC) terrain is straightforward. Staircase approximation is used to model non-flat longitudinal terrain profile in both simulators. It is achieved by forcing all tangential electric field components ( $E_x$  at vertical edges,  $E_z$  at horizontal edges for boundary cells and both for the inner cells) to be zero during the TDWP simulation. In TLM-WP, it is performed by using the short-circuit (SC) scattering matrix in the irregular terrain regions [3].

PEC boundary approximation is mostly adequate at upper VHF and above (i.e., frequencies higher than 100-150 MHz). On the other hand, accurate impedance boundary simulations are essential at HF frequencies and below. A propagator should be capable of handling imperfect surface effects including multi-mixed path propagation (e.g., land-sea transition). This is achieved by surface impedance modeling as explained in [14]. The first magnetic field component above the impedance boundary is calculated from its value at previous time-step plus two neighboring vertical and one horizontal electric fields by using surface impedance relation in terms of the resistance  $R_s$  and reactance  $L_s$  components [14]. It should be noted that the tangential electric and magnetic field components are related via a frequency-dependent surface impedance given in terms of frequency-dependent  $R_s$  and  $L_s$  values. On the other hand, their time-domain (TD) values are required in TDWP simulations. This makes a convolution process necessary in TD, which means extra computation time; therefore an approximation is implemented to eliminate the convolution process [5].

In TDWP implementations, the first magnetic field component above the impedance boundary is calculated from

$$\begin{aligned} H_y^{n+1/2}(i, k) = & \frac{1 - R_s \Delta t / 2\mu_0 \Delta x - L_s / \mu_0 \Delta x}{1 + R_s \Delta t / 2\mu_0 \Delta x - L_s / \mu_0 \Delta x} H_y^{n-1/2}(i, k) \\ & - \frac{\Delta t}{\mu_0 \Delta z (1 + R_s \Delta t / 2\mu_0 \Delta x - L_s / \mu_0 \Delta x)} [E_x^n(i, k+1) - E_x^n(i, k)] \\ & + \frac{\Delta t}{\mu_0 \Delta x (1 + R_s \Delta t / 2\mu_0 \Delta x - L_s / \mu_0 \Delta x)} [E_z^n(i+1, k)] \end{aligned} \quad (8)$$

instead of (5), while  $E_z$  on the surface is set to zero. In TLM-WP, incident and reflected voltage pulses are simulated at each time instant, but, field components are extrapolated and are used in handling impedance boundary condition similar to TDWP from (8).

Buildings, either as PEC obstacles or lossy structures are directly modeled by giving proper values to permittivity and conductivity.

It should be noted that preparation of TDWP algorithm, based on FDTD plus PML termination, is quite straightforward. On the other hand, one needs to introduce modifications in TLM-WP algorithm [3]. First of all, 2D TLM computation space is constructed via a series node representation (see Figure 2) to represent TM to z problem. Although four-arm node is shown in the figure, the fifth arm (with a short-circuit termination) is also used to model permeability of the node, which in turn represents permittivity because of the duality principle. Secondly, FDTD-PML algorithm, prepared for TDWP, is used in TLM-WP to absorb scattered fields [3-5]. In order to do that, a transition cell is located between TLM computation space and FDTD-PML blocks and field components of TDWP are matched to the voltage pulses of TLM-WP in this cell, unlike [15] where overlap cell is directly taken as the first cell in FDTD-PML region. Also, attention should be paid in matching FDTD fields to TLM voltage pulses at the left FDTD-PML-TLM interface, since FDTD field components in a cell are not symmetrically located as the voltages are in the TLM node. If for example,  $k=m$  (in the z-direction) is the overlap cell, then vertical electric field component ( $E_x$ ) of the next cell ( $k=m+1$ ) should also be used to write down TLM voltages in terms of FDTD fields (or vice versa).

The implementation of TD simulations is as follows:

- Source with a chosen spatial altitude distribution, having a pulse character in time (that yields broad band analysis with a single simulation) is injected via the necessary field components.
- Non-flat surface and/or buildings along a street are included from an input file.
- In order to implement non-homogeneous atmosphere, a refractivity profile over earth's surface (including earth's curvature) is introduced via relative permittivity of the air,  $\epsilon_r = n^2(x,z)$ .
- One-way propagation is traced via a 2D rectangular window. The content of this propagation window is the pulse that carries information related to terrain/building scattering, refractivity effects and surface losses.
- The propagation window moves from left to right in the computation space and circulates back to the left when reaches the right most-end, which is the initial profile of the next computation space.
- The process and TD simulations repeat until the wave longitudinally propagates to a desired range. The algorithm stores necessary information (such as range, terrain profile, transverse and/or longitudinal propagation characteristics at chosen observation points).
- Frequency domain characteristics may be obtained from the TD simulations by off-line discrete Fourier transformation (DFT) analysis.

### 3. Numerical Simulations

Both TDWP and TLM-WP have been applied to many complex propagation scenarios and validation and verification have been completed [1-5]. They also have been tested against other propagators based on analytical approximate formulations (such as hybrid ray-mode approach [16]) as well as frequency domain techniques (such as SSPE). Therefore they are not repeated here. Instead, the new propagators are applied to problems related to wireless propagation in rural and urban areas.

The results presented in this Section are either path loss vs. range/height or propagation factor vs. range/height. Path loss, as defined in (2), is reduced to

$$L_p(d) = 10 \log_{10} \left( \frac{P_t}{P_r(d)} \right) [dB], \quad (9)$$

when  $G_t$  and  $G_r$  are taken as 1 and system losses are left out (i.e,  $L_S = 1$ ). For excitation by a short electric dipole with a moment of  $M=5\lambda/2\pi$ , corresponding to  $P_t=1$  kW, the received power at a distance  $d$  can be determined from the computed field strength  $E$  via

$$P_r(d) = \frac{E_r(d)^2}{Z_0} \times \frac{\lambda^2}{4\pi}. \quad (10)$$

This leads to the expression

$$L_p(d) = 142.0 + 20 \log_{10}(f_{MHz}) - 20 \log_{10}(E_{\mu V/m}) [dB] \quad (11)$$

with the frequency and field strength measured in MHz and  $\text{dB}\mu\text{V/m}$ , respectively.

Propagation factor ( $E/E_0$ ) is simulated as pictured in Figure 3. First, the simulation is run for propagation over a given non-flat terrain and refractivity conditions, and  $E(t)$  vs. range (at constant height) or height (at a given range) is stored. For this run, top, left and right of the computation space are terminated with PML blocks (see Figure 3a). Then, the bottom boundary is removed and refractivity of air is taken, and simulation is repeated (see Figure 3b). In this case,  $E_0(t)$  vs. range (at constant height) or height (at a given range) is stored. In the second run, the whole computation space is terminated by PML blocks. Moreover, source and observer locations are shifted up until mid heights, so that unwanted reflections from the bottom PML block does not affect the results. Finally, the variations at multiple frequencies are obtained applying Fourier transform. The errors introduced by imperfect PML blocks cancel each other via this procedure.

### 3.1. Propagation in rural areas

The TDWP and TLM-WP propagators are first tested over smooth, spherical earth. The propagation region is characterised by longitudinally homogeneous, bi-linear vertical refractive index,  $n$ , with the gradient of  $dn/dx=10^{-3}$  [n unit/m]. The vertical distribution of the source is Gaussian with spatial extent  $\approx 15$  m and maximum at 26 m height (i.e., the vertical profile is non-zero between 18.5 m and 33.5 m). The temporal distribution is a once-differentiated Gaussian pulse with 200 MHz bandwidth centred at 200 MHz. A  $1000 \times 500$  FDTD/TLM computation (corresponding to  $100\text{m} \times 50\text{m}$  physical) space is used. A  $1000 \times 250$  virtual window circulates 20 times as if the longitudinal number of cells in FDTD/TLM computation space is 5000. As the wave propagates, it spatially extends because of cylindrical spreading, splits into upward and downward propagating waves because of bilinear refractivity profile, reaches the bottom surface and reflects back, giving rise to interference between the leading direct and trailing ground-reflected waves.

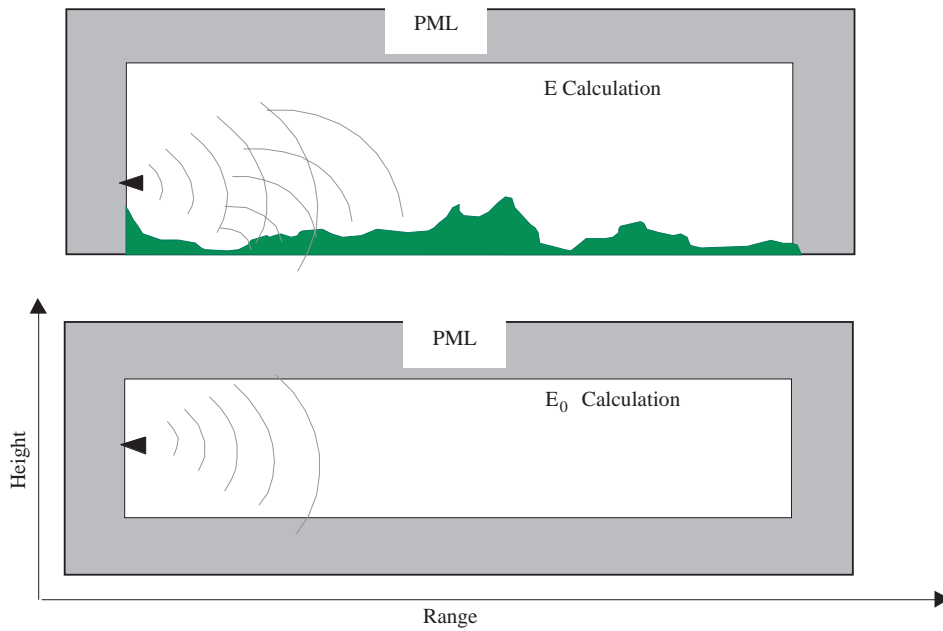


**Figure 3.** Scenario for numerical propagation factor simulations

Time histories of the pulse during propagation are accumulated at different ranges and along two constant heights, and are plotted in Figure 4, where the results of both are almost indistinguishable. In Figures 4a and 4b, the receiver heights are chosen to be 13 m and 35 m above the ground, respectively. Three plots correspond to the 94ns time histories (i.e., signal vs. time) at three different ranges. Since the scale in each plot is normalised to its maximum value in order to reveal the detailed pulse shapes along the entire trajectory, relative field strengths with respect to the first window are also included as dB values in the plots. At  $z=23.5\text{m}$ , only the initial pulses appear inside the 94ns propagation windows because the delay of the signal caused by the path difference (distance between direct and ground reflected pulses) exceeds the window length. As the distance increases, the path difference decreases and the ground-reflected pulse also appears inside the 94ns propagation windows, as shown in the second windows. Inside the last windows the direct and ground-reflected pulses are almost indistinguishable.

In order to predict path loss at a given range and given frequency, one should obtain frequency domain behaviours from TD simulation results. In order to do that;

- TD propagation data is accumulated at a number of altitude (range) points at the desired range (altitude). The accumulation continues until all the transients disappear at all observation points.
- After the TD simulation, altitude field distribution at any frequency (within the content of the pulse) is obtained by off-line DFT analysis.

Typical results are pictured in Figure 5, where TDWP and TLM-WP results are also compared with the SSPE propagator [1]. Here, a fictitious tri-linear vertical refractivity is chosen with refractive index gradients between ground and 15m, 15m-25m and above 25m as  $dn/dx=-1.2 \times 10^{-5}$ ,  $5 \times 10^{-6}$  and  $-1.2 \times 10^{-5}$ , respectively. The spatial distribution of the source is Gaussian at a height of 15 m, with spatial extent of  $\approx 12$  m. Temporal distribution is a once-differentiated Gaussian pulse in TLM-WP and TDWP. This short pulse has 200 MHz bandwidth centred at 200 MHz. The SSPE propagator, with the same spatial source distribution, is run separately for each frequency. With these parameters, energy is mostly trapped

along the surface and the pulse reaches to PML blocks at larger distances compared to standard atmosphere. Therefore, numerical dispersion effect is dominant in this example. The first two plots belong to the results at a range of 621.5 m reached at the 25<sup>th</sup> window (corresponding to  $311\lambda$  at 150 MHz and  $518\lambda$  at 250 MHz, respectively). At these ranges the propagating pulse is still confined in the sliding window and the agreement is very good. On the other hand, the last two figures belong to a range of 1121.5m reached at 45<sup>th</sup> window ( $561\lambda$  at 150 MHz and  $935\lambda$  at 250 MHz), where the sliding window is hardly capable of holding the propagating pulse. Although the sliding window hardly bounds all the forward-propagated energy, very good agreement may still be obtained in frequency domain as long as most of the dominant contribution is traced.

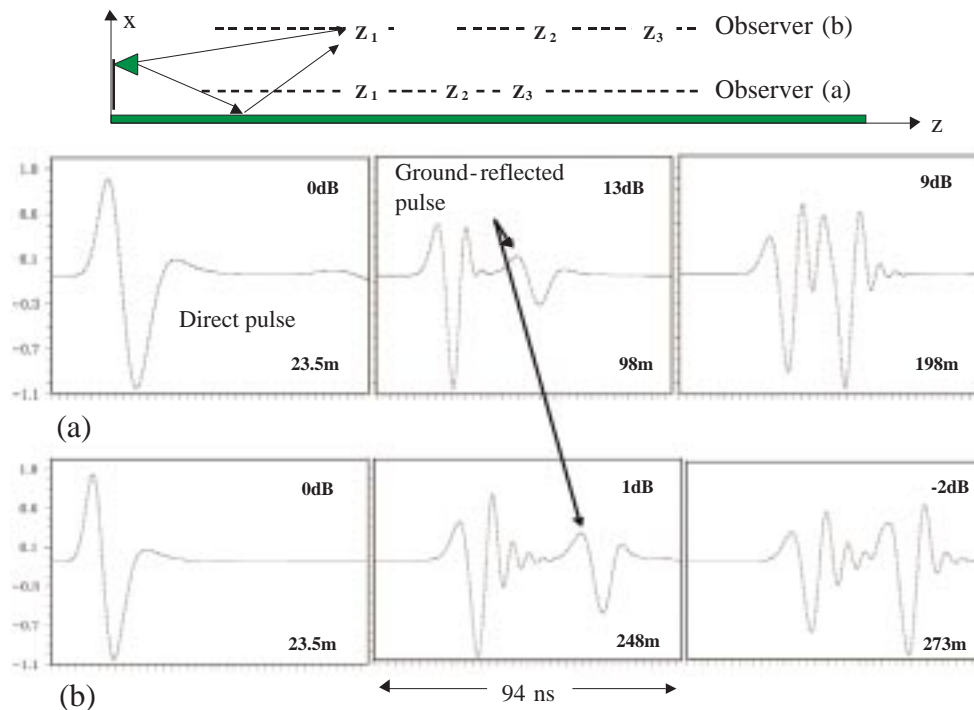


**Figure 4.** Time histories of the pulse in observed at different ranges along (a) 13 m, (b) 35 m above the surface; Solid: TLM-WP, dashed: TDWP, (vertical axis is normalized pulse amplitude).

TDWP and TLM-WP are tested against various different propagation scenarios, where non-flat terrain as well as multi-mixed paths are included, and it has been shown that these TD propagators can handle short and medium range (up to thousands of wavelengths at this stage with a PIII, 128MB RAM personal computer [1-5]). Therefore, they are not repeated here in detail. Only a comparison is given on a typical non-flat terrain as pictured in Figure 6. Here, a 1.5 km long non-flat terrain, with maximum height of 40 m) is taken into account (see Figure 6a). The source and observation points are 5 m above the ground and the mesh sizes are taken as 10cm.. Although SSPE does not include the back-scatter effects, TDWP and TLM-WP results contain local back-scatter contribution as long as it is within the sliding window. This explains the discrepancy between SSPE and TD propagators. As it is seen in Figure 6, there is also a discrepancy between the magnitudes of TDWP and TLM-WP, which is not observed for propagation over smooth ground. This can be because of numerical dispersion or differences in abilities of the FDTD and TLM implementations themselves resulting in different responses to the scattering mechanisms, such as reflection,

edge/tip diffraction, multi-path interference, surface waves, which is under investigation.

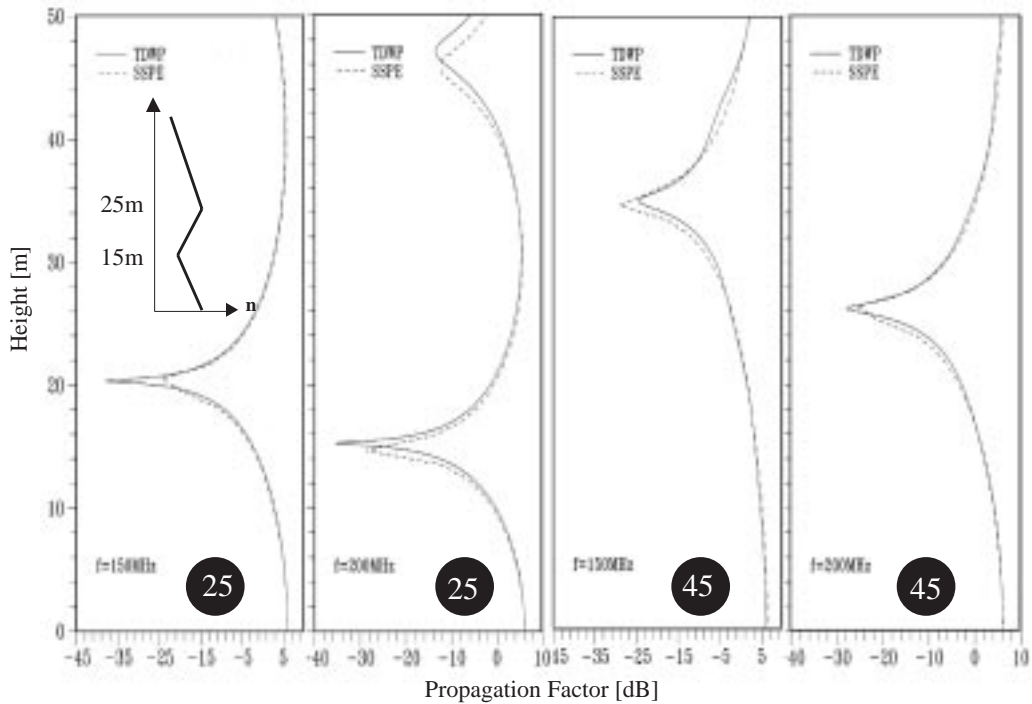


Figure 5. Propagation factor vs. height after 25 and 45 sliding windows.

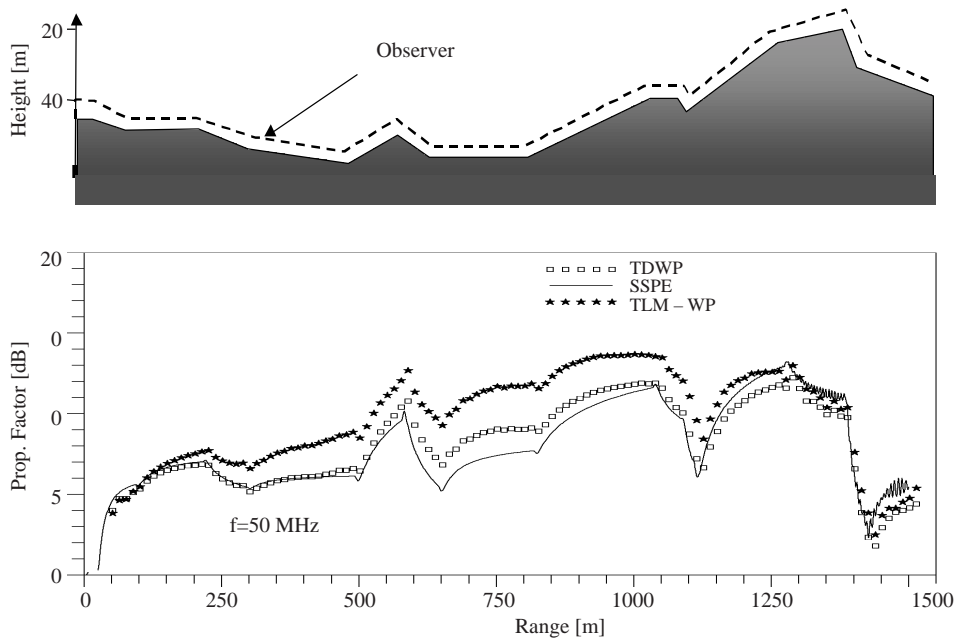


Figure 6. Propagation factor vs. range for the typical non-flat terrain

### 3.2. Propagation in urban regions

TD propagators are applicable in wireless communications when the depths of the buildings are assumed large enough to reduce the problem to a 2D case. Here, various scenarios that include nearby buildings are

taken into consideration.

The power of the TD propagators arises from their applicability in wireless communication in urban regions, such as along a narrow street with tall buildings in different sizes. In this section this is presented on various scenarios.

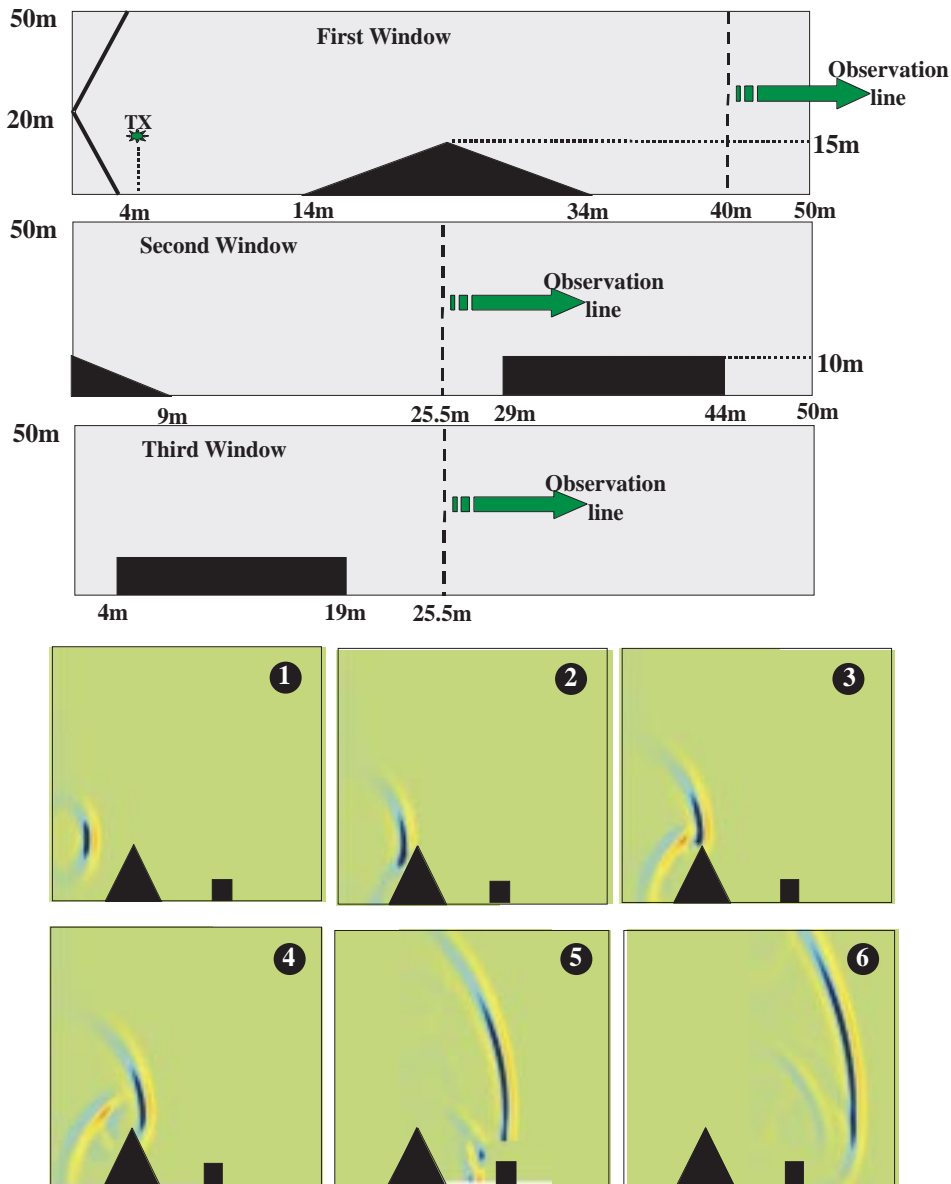


**Figure 7.** (Top) The first three consecutive sliding windows and their terrain contents, (bottom) TD forward and backward pulse scattering over different obstacles.

First, a scenario, where strong back-scatter effects occur, is taken into account. A 15 m high, 20 m long triangular building is located 10 m away from a pulse source. A 10 m high, 15 m long rectangular building is located 15 m after the first one. They are assumed to be PEC. The previous Gaussian pulse source is located at a height of 15 m. and temporal distribution is a once-differentiated Gaussian pulse with 100MHz bandwidth. The scenario and screen captures of TD pulse scattering at different ranges is given in Figure 7b (3 sliding windows are used in this example, as shown in Figure 7a). Since very similar results are

obtained, only TDWP results are pictured in this figure.

Vertical field distributions at three observation ranges, obtained at 50 MHz is plotted in Figure 8. Excellent agreement obtained at this frequency is clearly observed. It should be noted that neither SSPE nor analytical approximate techniques can handle this scenario, because of strong up and back scattering contributions.

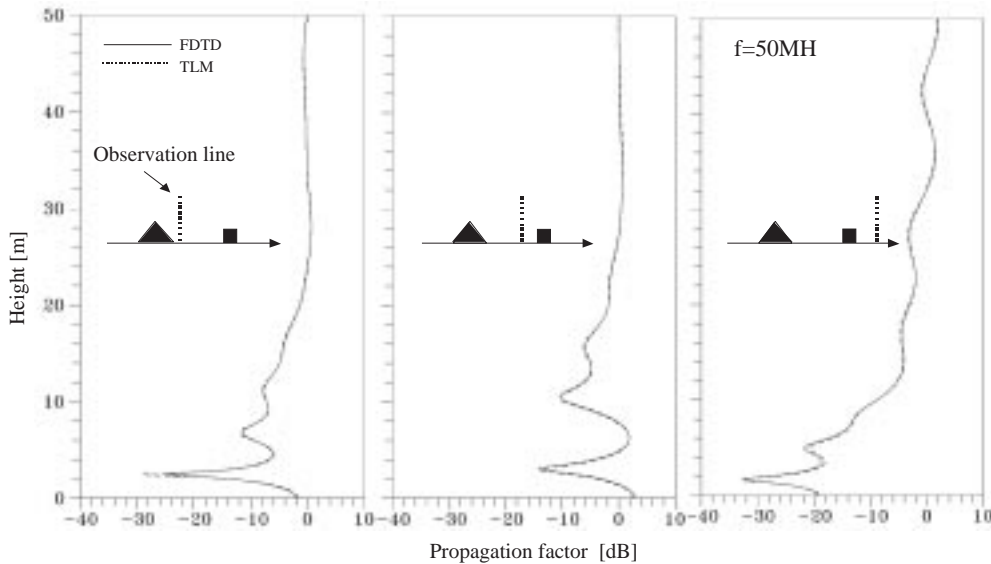


**Figure 8.** Propagation factor vs. height at three ranges ( $f=50$  MHz).

The maximum range can also be covered within a computation space for the scenario in Figure 7 and Figure 8. In this case, TDWP and TLM-WP reduce to FDTD and TLM, respectively, where all forward and backward scattered components are completely accumulated during the simulation in TD. In most of the practical problems maximum ranges of interest can not be covered by one or a few sliding windows. Therefore, while the sliding window is tracing the longitudinally propagating component, backward and upward propagated waves are also traced as long as they are confined inside the sliding window. There may still be backward and upward scattered contributions at observation points where the window has already passed. Because of this inefficiency, TD propagators are called to handle local back and up scattered components. In order to show these effects, a scenario in Figure 9 is taken into account. Here, two 15 m tall PEC triangular buildings having 10 m base lengths are separated with a distance of 25 m. The other dimensions and source and observation locations are mentioned in the figure. The mesh size,  $\Delta$ , is 10 cm in both TD simulators. The same Gaussian source is used and TD propagation along the buildings is simulated in two ways: (i) with unique FDTD and TLM spaces (without sliding), (ii) with two sliding windows. The results are given in Figure 10 (for 50 MHz) and Figure 11 (for 100 MHz) as propagation factor vs. height at four observation ranges and at two frequencies (it should be noted that these results belong to a single TD simulation plus multiple DFT application). In the figures, observation ranges from left to right are numbered from 1 (at 15 m) to 4 (at 70 m). Almost indistinguishable solid and dashed lines correspond to TDWP and TLM-WP computations, respectively, while the solid line with dots represents single window FDTD computations. It is clearly observed in these figures that, although TDWP and TLM-WP results have indistinguishable agreement, they do not agree very well with the FDTD, which may be assumed as a reference solution. Moreover, unacceptable discrepancies appear at some heights and ranges. Here, FDTD results represent reference solutions (since numerical dispersion ratios are 30 and 60 at 100MHz and 50

MHz, respectively), and the reason of the discrepancies may easily be understood from the scenario given in Figure 9. The strongest back and up scattered components are expected to be at the first observation range, at the bottom and at heights above the source (because of the inclined wall of the wedge type building). Not so strong as the dominant scatter, back and up scattered components are also expected in between the buildings. On the other hand, at the last observation range forward propagating wave is dominant, therefore, as expected, the best agreement is obtained at this range (see Figure 11).

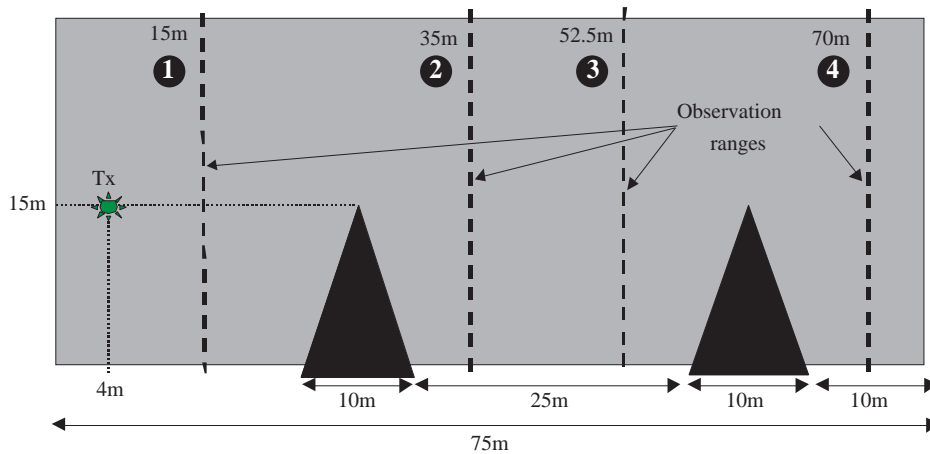


**Figure 9.** A scenario with two wedge shaped PEC obstacles (base=10m, height=15m). Transmitter is located 15 above the PEC ground.

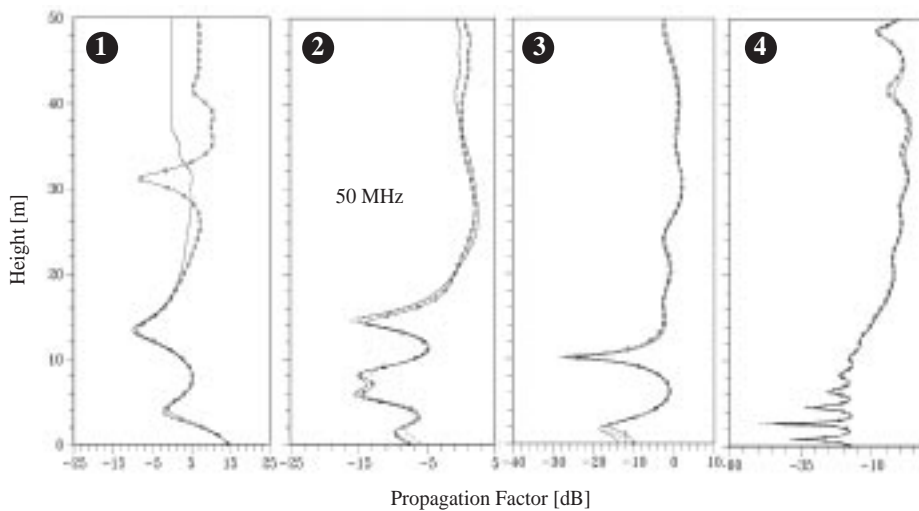


**Figure 10.** Propagation factor vs. height at 50 MHz at four observation ranges mentioned in Figure 9. Solid: TDWP, Dashed: TLM-WP, Solid with dots: FDTD.

Longitudinal variations of field strength are also calculated via TDWP and TLM-WP and are presented in Figure 12 (at 15 m height and for 50 MHz) and Figure 13 (at 15 m height and for 100 MHz). As seen, although range variations are highly oscillatory almost perfect agreement is obtained between TDWP and

TLM-WP results. It is also interesting to observe tip diffracted components (two peaks at ranges 25 m and 60 m, which correspond to the tips of the buildings) in 50 MHz figure.

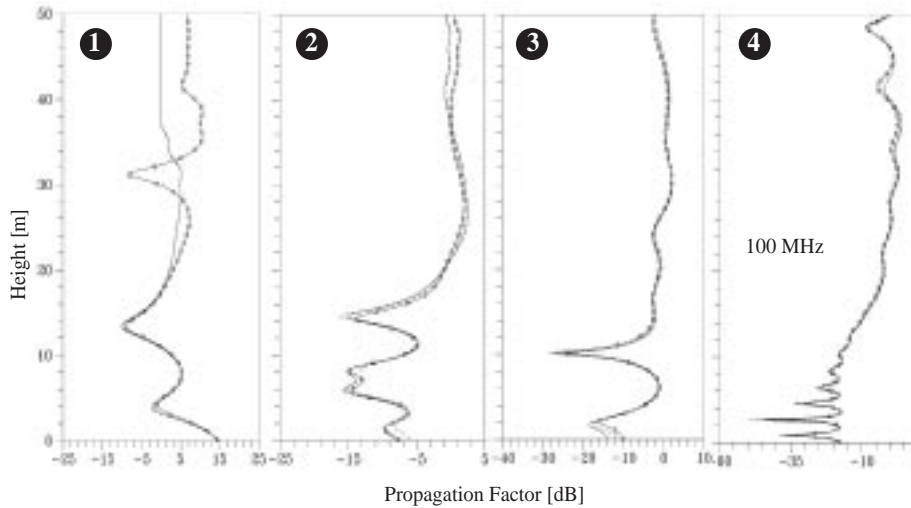


**Figure 11.** Propagation factor vs. height at 100 MHz at four observation ranges mentioned in Figure 9. Solid: TDWP, Dashed: TLM-WP, Solid with dots: FDTD.

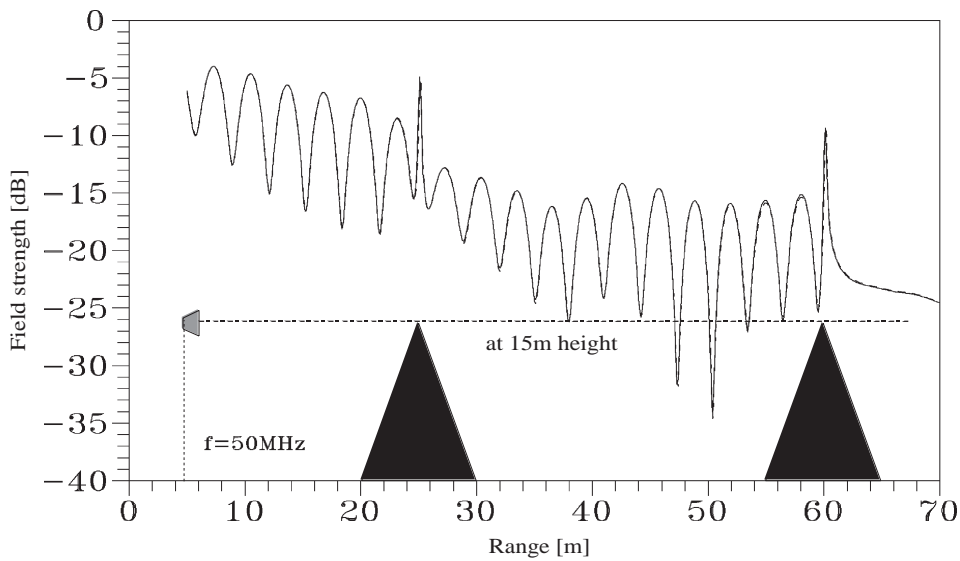


**Figure 12.** Normalized field strength vs. range at 15 m fixed height (at 50 MHz). Solid: TDWP, Dashed: TLM-WP.

Finally, a complex scenario, where four different shaped buildings with different sizes are used, is taken into account as given in Figure 14. Again, all dimensions and source/observation locations are mentioned in the figure. The buildings are assumed to be (i) PEC, (ii) empty with lossy walls (each building has two-cell walls with  $\sigma=0.01$  S/m and  $\epsilon_r=4.0$ ). The results are presented in Figure 15 and 16, for the cases (i) and (ii) respectively, as propagation factor vs. height at given four observation ranges. Both TDWP and TLM-WP computations are carried out within a unique FDTD/TLM computation space (to account

for all scattered contributions). As shown in Figure 15, the results of TDWP and TLM-WP do not agree very well as observed in the previous examples. There is no discretization error in this example, since all the buildings are chosen to be rectangular. Possible sources of these discrepancies are (i) numerical dispersion errors (it may require numerical dispersion ratios higher than 30 at 100 MHz), (ii) PML termination (since the scattering mechanisms, such as reflection, edge/tip diffraction, multi-path interference, surface waves, etc, become complex in this example), or (iii) differences in abilities of the FDTD and TLM implementations themselves. In Figure 16, TDWP results are presented together when buildings are PEC and lossy. It is observed that the loss of buildings do not influence the field strengths above the buildings, but, certainly weakens along the streets up to building heights. There is also discrepancy at heights above the buildings because of the diffraction effects. As much as 25 dB to 30 dB signal attenuation should be expected along the streets in scenarios similar to the one presented here. The situation is clearly pictured in Figure 17, where propagation factor vs. range is plotted at 15 m constant height.

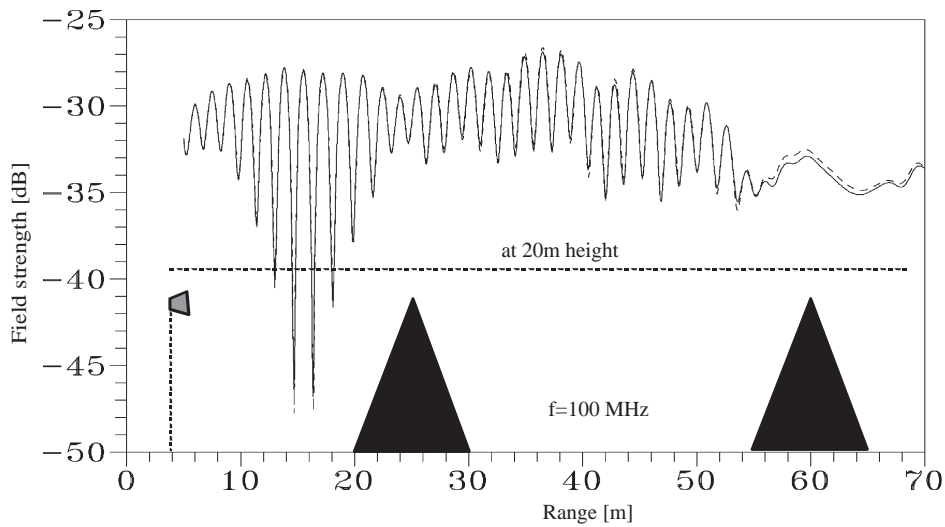


Figure 13. Normalized field strength vs. range at 20 m fixed height (at 100 MHz). Solid: TDWP, Dashed: TLM-WP.

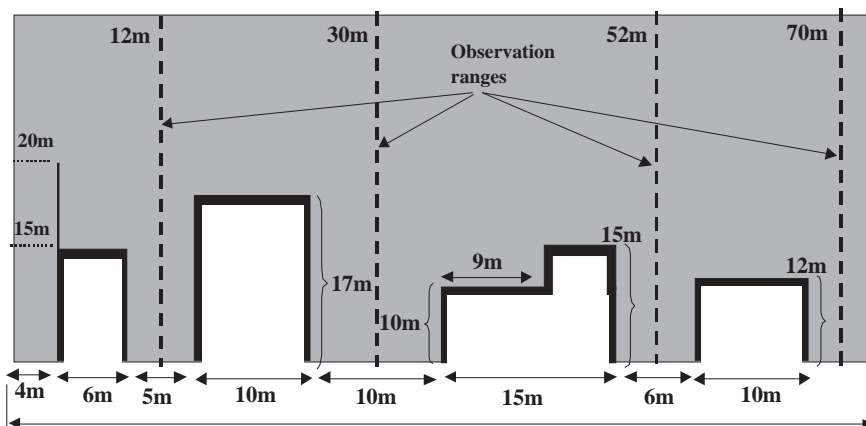
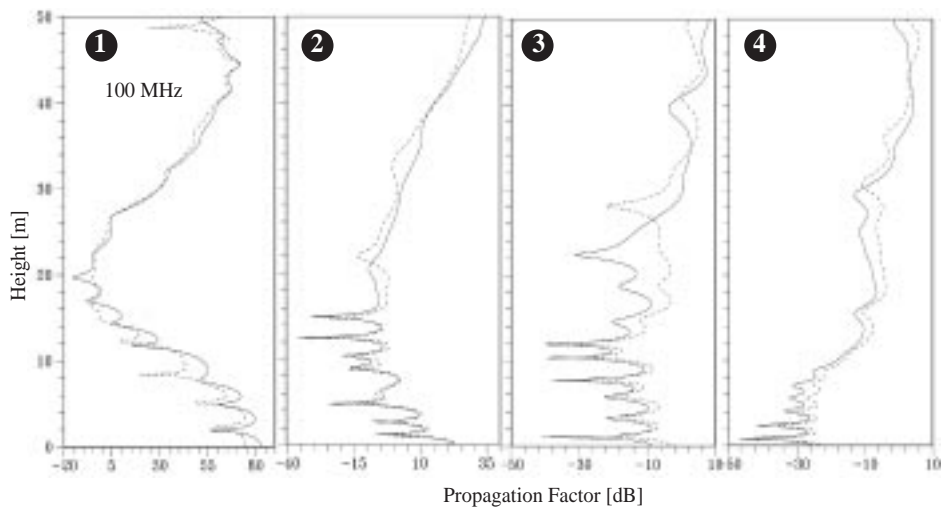
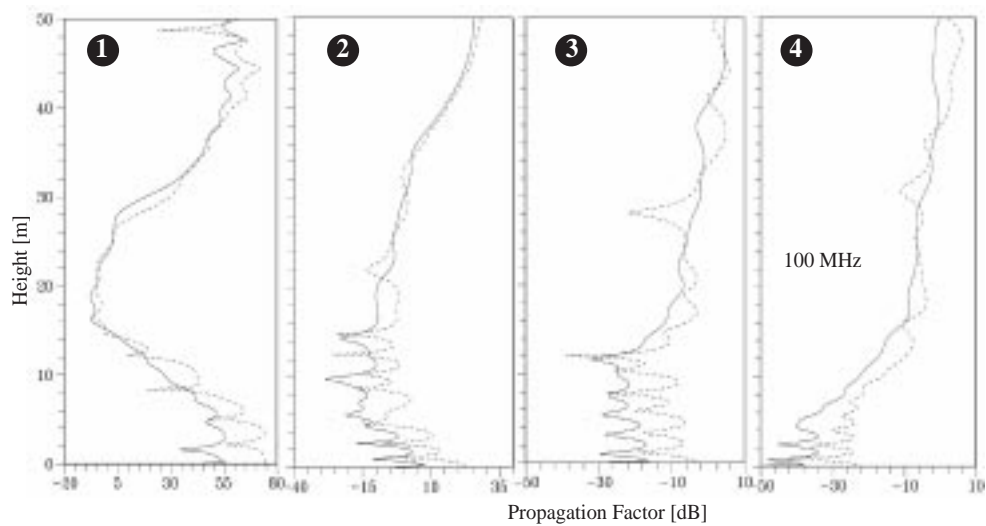


Figure 14. A scenario with multiple buildings and four observation ranges. The transmitter is located at top of the first building (i.e., 20 m above ground).



**Figure 15.** Propagation factor vs. height at 100 MHz at four observation ranges mentioned in Figure 14, when buildings are all assumed PEC. Solid: TDWP, Dashed: TLM-WP.



**Figure 16.** Propagation factor vs. height at 100 MHz at four observation ranges mentioned in Figure 14, when buildings are lossy (each building has two-cell lossy walls with  $\sigma=0.01$  S/m and  $\epsilon_r=4.0$  and inside is air). Solid: TDWP (for lossy buildings), Dashed: TDWP (for buildings all assumed PEC)

The beauty of the TD simulators resides in a fact that they visualize the pulse scattering mechanism directly in TD. Last example, belongs to the scenario given in Figure 14, where snapshots at different time instants are plotted in Figure 18 as signal strength vs. range-height. The multi-reflections, edge and tip diffraction and ringing in between buildings are clearly observed in the figure.

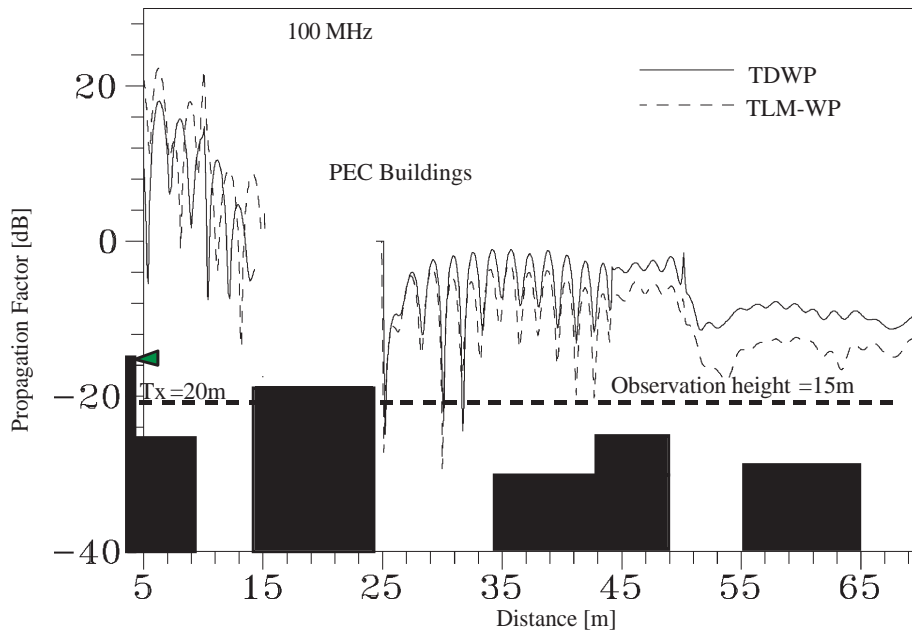


**Figure 17.** Propagation factor vs. range at 15 m constant height at 100 MHz, when buildings are all assumed PEC. Solid: TDWP, Dashed: TLM-WP.

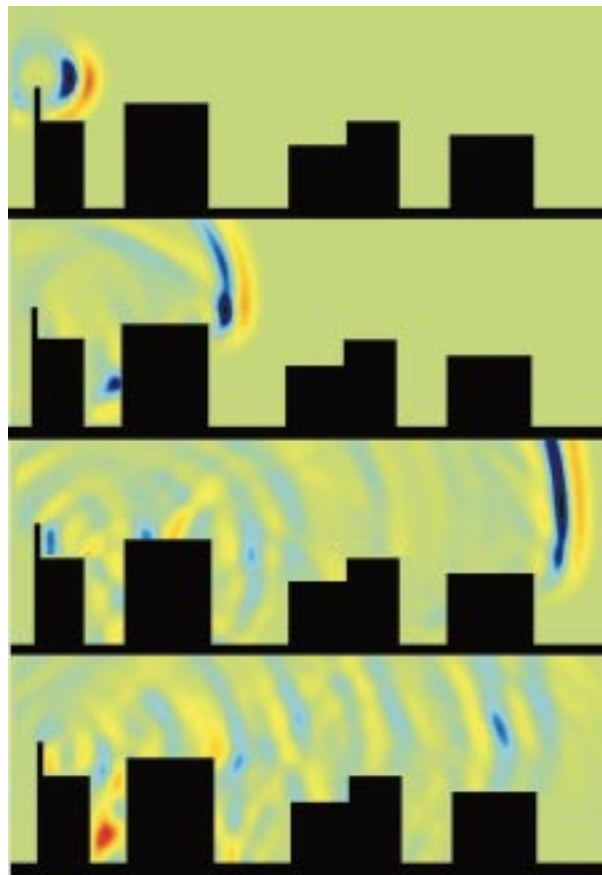


**Figure 18.** A 3D picture of pulse scattering along the streets with buildings mentioned above.

## 4. Conclusions and Discussions

The two novel time domain wave propagators that were recently introduced are used in simulating path loss prediction in both rural and urban area GSM cellular coverage. TDWP and TLM-WP are compared on complex propagation scenarios, and very good agreement is obtained. These new propagators are demonstrated to be capable of simulating different wave phenomena over realistic earth's surface (including non-flat terrain and imperfect ground effects) in rural regions as well among the tall buildings (highrise), which are modeled as both PEC and lossy obstacles.

The new time domain wave propagators have three major restrictions; high power computer requirements, numerical dispersion effects and unwanted reflections from PML terminations. Obviously, the first restriction may be overcome by increasing computer memory size and CPU speed. The more powerful computer we have the larger computation space as well as the larger sliding window. As the pulse, trapped inside the sliding window, is propagated towards the desired range along the chosen path it enlarges and interferes with specularly reflected and/or other diffracted components, and it becomes hardly possible to keep it inside the window. The range of application may also be extended depending on the available computer facilities. Moreover, path loss prediction for lower and center frequencies of the pulse frequency band may still be extracted from the dispersed pulse as long as the main propagating pulse can be kept inside the sliding window. Finally, the third restriction, unwanted, non-physical reflections along PML interface may be reduced by increasing number of PML cells, which in turn also require high power, large memory computers.

Nevertheless, both TDWP and TLM-WP propagators are very promising and seem to be powerful tools in simulating macro and mini cell planning in rural and urban areas. Their capabilities in reaching longer ranges may certainly be increased by using parallel processing techniques and/or dynamic sliding window sizes.

## References

- [1] L. Sevgi, F. Akleman, L. B. Felsen, "Ground Wave Propagation Modeling: Problem-Matched Analytical Formulations And Direct Numerical Techniques", (to appear in *IEEE-AP Magazine*)
- [2] F. Akleman & L. Sevgi, "A Novel Time-domain Wave Propagator", *IEEE Transactions on Antennas and Propagat.* Vol. 48, No 5, pp.839-841, May 2000
- [3] M. O. Ozyalcin, F. Akleman and L. Sevgi, "A TLM Based Novel Time Domain Ground Wave Propagator", (submitted to) *IEEE Transactions on Antennas and Propagat.* May 2001
- [4] F. Akleman & L. Sevgi, "Realistic Surface Modeling in a Time-domain Wave Propagator", *IEEE Transactions on Antennas and Propagation*, (major revision) Feb 2001
- [5] F. Akleman, M.O. Ozyalcin & L. Sevgi, "Time Domain Ground Wave Propagators based on FDTD and TLM Techniques", CEM-TD, Proc. of 4<sup>th</sup> Int. Workshop on CEM in the Time Domain – FDTD, TLM and Related Techniques, pp.97-104, Sep 16-19 2001, Nottingham, UK
- [6] Y. Okumura, E. Ohmori, T. Kawano, and K. Fukuda, "Field Strength and its variability in VHF and UHF land mobile radio service." *Rev: Elec. Commun. Lab.*, vol. 16, nos. 9-10. Sept.-Oct., 1968
- [7] M. Hata, "Empirical formula for propagation loss in land mobile radio services", *IEEE Trans. Veh. Technol.*, vol. VT-29, pp. 317-325, Aug. 1980

- [8] K. Bullington, "Radio propagation for vehicular communications," *IEEE Trans. on Veh. Technol.*, vol. vt-26, no. 4, Nov. 1977
- [9] J. Walfisch and H. L. Bertoni, "A theoretical model of UHF propagation in urban environments", *IEEE Trans. Antennas. Propagat.*, vol. 36, no. 12. Dec., 1988
- [10] G. K. Chan, "Propagation and coverage prediction for cellular radio systems", *IEEE Trans. Veh. Technol.*, vol. 40, no.4, Nov. 1991
- [11] M. J. Neve, and G. B. Rowe, "Mobile radio propagation prediction in irregular cellular topographies using ray methods," *IEEE Proc.-Microw. Antennas Propag.*, Vol. 142, December 1995
- [12] K. S. Yee, "Numerical solution of initial boundary value problems involving Maxwell's equations" *IEEE Transactions on Antennas and Propagat*, V-14, no. 3, pp. 302-307, 1966
- [13] C. Christopoulos, *The transmission-line modeling method*, Oxford: Oxford University press, 1995
- [14] J. H. Beggs, R. J. Luebbers, K. S. Yee, K. S. Kunz, "Finite-Difference Time-Domain Implementation of Surface Impedance Boundary Conditions", *IEEE Transactions on Antennas and Propagat*, Vol:40 No:1, January 1992
- [15] C. Eswarappa and W. J. R. Hofer, "Implementation of Berenger Absorbing Boundary Conditions in TLM by Interfacing FDTD Perfectly Matched Layers", *Electronic Letters*, Vol. 31, No. 15, 1995
- [16] L. Sevgi & L. B. Felsen, "A new Algorithm for Ground Wave Propagation Based on a Hybrid Ray-Mode Approach", *Int. J. of Numerical Modeling*, Vol.11, No 2, pp.87-103, March 1998
- [17] R. J. Luebbers, "Finite conductivity uniform GTD versus knife-edge diffraction in prediction of propagation path loss," *IEEE Trans. Antennas Propagat.*, vol. AP-32, pp. 70-76, Jan. 1984